# Density Field Dynamics and Its Variant Extensions: A Constrained Flat-Background Optical-Medium Family

Gary Thomas Alcock

October 3, 2025

**Abstract**

**We present Density Field Dynamics (DFD), a flat-background optical-medium framework that is fully consistent with existing tests of general relativity yet decisively falsifiable by near-term laboratory experiments.** DFD introduces a scalar refractive index $n = e^{\psi}$ that governs both light propagation and inertial dynamics. From a convex aquadratic scalar action, the crossover function $\mu(x)$ emerges non-adhoc: $\mu \to 1$ reproduces Newtonian/PPN limits in high gradients, while the deep-field limit yields MOND-like scaling. Two sharp laboratory discriminators follow: (1) *non-null cavity–atom frequency slopes* across gravitational potentials, originating from mild differential scalar dressing of $\{\alpha, m_e, m_p\}$ in a verified nondispersive band; and (2) a $T^3$ *contribution* to matter-wave interferometer phases, even in $k_{\mathrm{eff}}$ and rotation-odd, within reach of long-baseline instruments. We map six bounded extensions (electromagnetic back-reaction, dual-sector $(\epsilon/\mu)$ split, nonlocal kernels, vector anisotropy, stochasticity, strong-field closure) that address anomalies while reducing to the same base dynamics. Beyond the laboratory and solar system, DFD embeds a transverse–traceless spin-2 sector with $c_T$=1 and GR polarizations, reproduces black-hole/shadow observables via optical geodesics of $n = e^{\psi}$, and supplies a minimal cosmology module in which distance biases and $H_0$ anisotropies map directly onto an effective $w_{\mathrm{eff}}(z)$ without a dark-energy fluid. Linear growth remains near–ΛCDM at $z \gtrsim 1$, while late-time departures are testable through distance duality and $H_0$–foreground correlations. **Thus DFD is conservative where tested and bold where testable, with concrete predictions from precision clocks to gravitational waves, black-hole optics, and cosmology.** We also give a minimal strong-field closure (DFD–TOV plus TT dynamics) yielding immediate, testable forecasts for mass–radius relations, optical shadows, and merger waveforms.

## 1 Introduction

Einstein's general relativity (GR) geometrizes gravitation as spacetime curvature. Yet alternatives remain viable, from scalar–tensor theories [1] to $f(R)$ models [2] and Einstein–æther theories [3]. If one restricts attention to flat Minkowski spacetime while maintaining an invariant two-way light speed, then a natural minimal class emerges: *refractive* or *optical-medium* theories, where gravity manifests through a scalar index field controlling rods, clocks, and phases. This aligns with scalar frameworks [5, 6] and analog-gravity constructions [4].

The motivation for DFD is not metaphysical elegance but *experimental falsifiability*. Two sharp discriminators appear immediately:

1. **Cavity–atom Local Position Invariance (LPI) slope:** GR predicts a strict null in the *ratio* of cavity to atomic frequencies across potential differences (within standard PPN and composition-independence assumptions [8, 7, 9, 25]). DFD predicts a non-null slope under operational conditions defined below ("nondispersive band"), sharpened in the dual-sector extension.

2. **Matter-wave interferometry:** DFD predicts a small but testable $T^3$ contribution to the phase, absent in GR at leading order.

*Finally, we provide concise but quantitative predictions in the remaining sectors*—gravitational waves *(embedded TT spin-2 with $c_T = 1$)*, black holes/shadows *(optical geodesics), and* cosmology *(distance bias and $H_0$ anisotropy)—so the proposal is complete across observational domains.*

# 2 Base Density Field Dynamics

## 2.1 Field equations

DFD postulates a scalar refractive field $\psi$ such that

$$n = e^{\psi}, \tag{1}$$

so that geometric optics is governed by Fermat's principle in $n$, while matter accelerates according to

$$\mathbf{a} = \tfrac{c^2}{2}\,\nabla\psi. \tag{2}$$

**General sourcing law (global).** Allowing a single crossover function $\mu$ between high-gradient (solar) and deep-field (galactic) regimes, the scalar obeys

$$\nabla\cdot\Big[\mu\big(|\nabla\psi|/a_\star\big)\,\nabla\psi\Big] = -\,\frac{8\pi G}{c^2}\,(\rho-\bar\rho), \tag{3}$$

with $\mu\to 1$ in the solar/high-gradient regime and $\mu(x)\sim x$ in the deep-field regime.

**Local reduction (solar/laboratory).** In laboratory and solar-system applications, $\mu \to 1$ and the uniform background $\bar\rho$ contributes only a constant offset to $\psi$ that drops out of local gradients; thus

$$\nabla^2\psi = \frac{8\pi G}{c^2}\,\rho, \tag{4}$$

so that $\psi = 2\Phi/c^2$ with $\Phi$ the Newtonian potential. Equation (4) is the local, Poisson-like sourcing law; the nonlocal kernel variant generalizes this, and Eq. (3) governs deep-field/cosmological optics.

**Action principle and crossover motivation.** A convenient origin for the crossover law is an aquadratic (k-essence–like) action for the scalar,

$$S_\psi \;=\; \frac{a_\star^2 c^2}{8\pi G}\int d^3x\,dt\;F\Big(\frac{|\nabla\psi|^2}{a_\star^2}\Big)\;-\;\int d^3x\,dt\;\psi\,\frac{8\pi G}{c^2}(\rho-\bar\rho), \tag{5}$$

with $F$ a dimensionless, convex function. Varying (5) gives

$$\nabla\cdot\Big[\mu(X)\,\nabla\psi\Big] \;=\; -\,\frac{8\pi G}{c^2}(\rho-\bar\rho), \qquad \mu(X)\;\equiv\;F'(X), \quad X\equiv\frac{|\nabla\psi|^2}{a_\star^2}. \tag{6}$$

Thus $\mu$ is not *ad hoc* but the derivative of the scalar kinetic function. Physical requirements:

- *Stability/positivity:* $F'(X)>0$ and $F''(X)\geq 0$ (no ghosts; elliptic operator).
- *High-gradient limit:* $X\gg 1 \Rightarrow \mu\to 1$ (Poisson/PPN recovery).
- *Deep-field limit:* $X\ll 1 \Rightarrow \mu(X)\propto X^{1/2}$ or $X$ to generate RAR/MOND-like scaling in galaxies.

Two minimal families used in fits are

$$\text{(simple)}\quad \mu(x)=\frac{x}{1+x},\qquad \text{(standard)}\quad \mu(x)=\frac{x}{\sqrt{1+x^2}},\qquad x\equiv\frac{|\nabla\psi|}{a_\star}. \tag{7}$$

The scale $a_\star$ is fixed phenomenologically by the baryonic RAR; solar-system and laboratory domains have $x\gg1$, so $\mu\to1$ and Eq. (4) follows. The convex $F$ gives a well-posed boundary-value problem and guarantees a unique weak-field limit consistent with PPN.

**Crossover motivation.** This crossover is not introduced ad hoc but arises generically from any convex aquadratic scalar action. The same functional structure underlies the Bekenstein–Milgrom AQUAL formulation; our choice of $F(X)$ simply specifies a minimal convex generator. Thus the $\mu(x)$ law should be viewed as phenomenology-anchored but variationally derived, guaranteeing well-posedness and recovery of both PPN and MOND-like branches without arbitrary interpolation.

### 2.2 Weak-field predictions

From (4) one recovers:

- **Newtonian limit:** $\mathbf{a}=-\nabla\Phi$.
- **Gravitational redshift:** $\Delta f/f=\Delta\Phi/c^2$.
- **Light bending:** Fermat's principle yields $\alpha=4GM/(bc^2)$ (Appendix A), reproducing GR's factor of two.
- **Shapiro delay and perihelion precession:** match GR at 1PN order [7].
- **PPN parameters:** $\gamma=1,\ \beta=1$ in the standard tests, matching GR at this level [7].

### 2.3 Laboratory discriminators

**Operationally nondispersive band (precision definition).** By a *nondispersive band* we mean a frequency range $\mathcal{B}$ around the cavity/clock operating frequencies such that

$$\left|\frac{\partial n}{\partial\omega}\right|_{\mathcal{B}}\ll\frac{1}{\omega}\quad\text{and}\quad\left|\frac{\Delta n}{n}\right|_{\mathcal{B}}\lesssim\mathcal{O}(10^{-15})\ \text{over the measurement bandwidth.} \tag{8}$$

This ensures phase and group velocities coincide to the precision needed for LPI comparisons, so the cavity frequency shift tracks $n=e^{\psi}$ without dispersive contamination.

**Base-DFD LPI mechanism (explicit).** Within a verified nondispersive band $\mathcal{B}$, let the cavity resonance obey

$$\frac{f_{\rm cav}}{f_{\rm cav,0}}=e^{\psi}, \tag{9}$$

while the co-located atomic transition responds *operationally* as

$$\frac{f_{\rm at}}{f_{\rm at,0}}=e^{\psi'}, \tag{10}$$

where $\psi'$ need not equal $\psi$ (a solid's optical path and an internal atomic interval can couple differently to the scalar field in an effectively nondispersive band). The measured ratio then acquires a slope

$$\frac{f_{\rm cav}}{f_{\rm at}}=\frac{f_{\rm cav,0}}{f_{\rm at,0}}\,e^{\psi-\psi'}\quad\Rightarrow\quad\frac{\Delta(f_{\rm cav}/f_{\rm at})}{(f_{\rm cav}/f_{\rm at})}=\Delta(\psi-\psi'), \tag{11}$$

which is *geometry-locked* via $\Delta\Phi/c^2$ along the height change. In the dual-sector extension below, $\psi-\psi'$ becomes parametrically larger because $\epsilon$ and $\mu$ respond oppositely, sharpening the discriminator.

**LPI slope test.** In GR, both atoms and cavities redshift as $\Delta f/f = \Delta\Phi/c^2$, so their *ratio* is constant (strict null). In base DFD, the small difference $\psi - \psi'$ above yields a non-null ratio slope. For ground-to-satellite $\Delta\Phi \sim 5 \times 10^7$ m$^2$/s$^2$, this gives $\Delta f/f \sim 5 \times 10^{-10}$. Current ratio bounds are at $\sim 10^{-7}$ [10, 11], leaving discovery space.

**Matter-wave interferometry.** In addition to the GR term $\Delta\phi \sim k_{\rm eff}\, g\, T^2$, DFD predicts a $T^3$ correction arising from gradient variations in $\psi$ (Appendix B). This correction is even in $k_{\rm eff}$ and rotation-odd, providing a discriminator. Estimated magnitude near Earth is $\sim 10^{-2}$ rad for $T \sim 1$ s, within reach of long-baseline interferometers and planned 10–100 m facilities [12, 13, 14, 15, 16].

**Microphysical origin of $\psi \neq \psi'$ (why atoms and cavities differ).** Operationally, the cavity frequency tracks the optical path $nL$ in a verified nondispersive band, so $\Delta \ln f_{\rm cav} = \Delta\psi$. Atomic transitions depend on the Rydberg scale and nuclear/Zeeman/hyperfine splittings:

$$\Delta \ln f_{\rm at} = K_\alpha\, \Delta \ln \alpha \;+\; K_{m_e}\, \Delta \ln m_e \;+\; K_{m_p}\, \Delta \ln m_p \;+\; \cdots , \tag{12}$$

with dimensionless sensitivity coefficients $K_i$ (order unity for many optical transitions). A minimal DFD completion allows mildly different scalar dressings for the electromagnetic and fermionic sectors,

$$\alpha(\psi) = \alpha_0\, e^{\lambda_\alpha \psi}, \qquad m_e(\psi) = m_{e0}\, e^{\lambda_e \psi}, \qquad m_p(\psi) = m_{p0}\, e^{\lambda_p \psi}, \tag{13}$$

consistent with the dual-sector ($\epsilon/\mu$) split (which fixes $c$ while permitting opposite $\epsilon, \mu$ responses). Then (12) gives

$$\Delta \ln f_{\rm at} = \Big( K_\alpha \lambda_\alpha + K_{m_e} \lambda_e + K_{m_p} \lambda_p + \cdots \Big)\, \Delta\psi \;\equiv\; \Delta\psi', \tag{14}$$

so the slope in the ratio is

$$\Delta \ln\!\left( \frac{f_{\rm cav}}{f_{\rm at}} \right) = \Delta(\psi - \psi') \;=\; \Big[ 1 - \big( K_\alpha \lambda_\alpha + K_{m_e} \lambda_e + K_{m_p} \lambda_p + \cdots \big) \Big] \Delta\psi. \tag{15}$$

Equivalence-principle tests (e.g. MICROSCOPE) bound *composition-dependent* combinations, but an *operational* LPI difference between an optical path and an internal atomic interval at the $10^{-9}$–$10^{-10}$ gravitational slope is still allowed once the measurement band is nondispersive and composition systematics are controlled. In the dual-sector variant, $\lambda_\alpha$ is naturally enhanced while $c$ remains invariant, strengthening the predicted non-null slope.

**Status of $\psi \neq \psi'$ coefficients.** The coefficients $\{\lambda_\alpha, \lambda_e, \lambda_p\}$ are bounded only indirectly by current equivalence–principle tests and remain open at $\mathcal{O}(1)$. In practice this is advantageous: the cavity–atom slope experiment itself directly calibrates these couplings. Across a plausible range $0.1 \lesssim \lambda \lesssim 10$, the predicted non-null slopes span $10^{-11}$–$10^{-9}$, fully within reach of next-generation missions. Thus the $\psi \neq \psi'$ mechanism is not a vulnerability but a calibration target to be pinned down experimentally.

## 3 Transverse–traceless (TT) gravitational waves within the optical ansatz

Within the same optical structure, promote the spatial sector to carry TT fluctuations,

$$g_{00} = -e^{\psi}, \qquad g_{ij} = e^{-\psi}\big(\delta_{ij} + h_{ij}^{\rm TT}\big), \quad \partial_i h_{ij}^{\rm TT} = 0, \quad h^{i}{}_{i}^{\rm TT} = 0. \tag{16}$$

Expanding the DFD scalar action to quadratic order in $h_{ij}^{\rm TT}$ yields the unique local kinetic term

$$S_{TT} = \frac{c^4}{64\pi G}\int dt\, d^3x\, \left[\tfrac{1}{c^2}(\partial_t h_{ij}^{\rm TT})^2 - (\nabla h_{ij}^{\rm TT})^2\right], \tag{17}$$

so the wave speed is $c_T = 1$. The sourced wave equation is

$$(\partial_t^2 - c^2\nabla^2)h_{ij}^{\rm TT} = \frac{16\pi G}{c^2}\left(T_{ij}^{({\rm m}),{\rm TT}} + \Pi_{ij}^{(\psi),TT}\right), \tag{18}$$

where $T_{ij}^{({\rm m}),{\rm TT}}$ is the TT projection of the matter stress and $\Pi_{ij}^{(\psi),TT}$ the near-zone $\psi$ stress. Compact binaries therefore radiate the two GR-like quadrupolar polarizations at leading PN order with $c_T = 1$ [23, 24]. Any DFD-specific amplitude/phase corrections enter through $\Pi_{ij}^{(\psi),TT}$ and are PN-suppressed; parametrically,

$$\left.\frac{\delta h}{h}\right|_{\rm DFD} \sim \kappa_\psi \left(\frac{v}{c}\right)^4, \qquad \kappa_\psi = \mathcal{O}(1), \tag{19}$$

i.e., $\gtrsim$2PN relative to the GR quadrupole, consistent with current bounds.

# 4 Black holes and shadows in DFD optics

In the optical-metric viewpoint, null rays follow Fermat geodesics of $n = e^{\psi}$. For a static, spherically symmetric source with $\psi(r) = 2GM/(c^2 r)$ in the high-gradient regime, the conserved impact parameter is $b = n(r)\, r \sin\theta$. The shadow boundary follows from the unstable circular-ray condition $d(b/r)/dr = 0$. To leading order this reproduces the GR photon-sphere location and thus shadow diameter within present EHT tolerances [22]. Deviations trace back to strong-field closure of $\psi$; demanding consistency with the observed M87* ring size implies an $\mathcal{O}$(few%) tolerance on any high-$\psi$ closure parameters. This furnishes a quantitative, minimal BH/shadow sector pending a full non-linear strong-field completion.

# 5 Variant Extensions of DFD

All variants reduce to base DFD but add refinements. (These variants are modular; none are required for the TT wave sector, black-hole optics, or the minimal cosmology module developed here.)

## 5.1 Electromagnetic back-reaction

Electromagnetic energy sources $\psi$, potentially destabilizing high-$Q$ cavities [17, 18].

## 5.2 Dual-sector $(\epsilon/\mu)$ split

$\psi$ couples differently to electric and magnetic energy:

$$\epsilon = \epsilon_0\, e^{f(\psi)}, \qquad \mu = \mu_0\, e^{-f(\psi)}, \tag{20}$$

so that $\epsilon\mu = 1/c^2$ remains invariant. A concrete choice that is both minimal and sufficiently general for small fields is

$$f(\psi) \;=\; \lambda\,\psi \;+\; \frac{\kappa}{2}\,\psi^2 \;+\; \mathcal{O}(\psi^3), \tag{21}$$

with $|\kappa\,\psi| \ll 1$ on laboratory scales. Then

$$\frac{\Delta\epsilon}{\epsilon} \simeq \lambda\,\Delta\psi \;+\; \kappa\,\psi\,\Delta\psi, \qquad \frac{\Delta\mu}{\mu} \;\simeq -\,\lambda\,\Delta\psi \;-\; \kappa\,\psi\,\Delta\psi, \tag{22}$$

so the two sectors respond oppositely at linear order (controlled by $\lambda$) with a tunable nonlinear correction (controlled by $\kappa$). Atoms and cavities then redshift differently, consistent with resonant anomaly searches [19]. For the linear case $f(\psi) = \lambda\psi$ one has $\Delta\epsilon/\epsilon \simeq \lambda\,\Delta\psi \simeq 2\lambda\,\Delta\Phi/c^2$, which is $\sim 10^{-9}$ at lab scales for $\lambda \sim \mathcal{O}(1)$, and can be amplified or suppressed by $\kappa$ in (21).

### 5.3 Nonlocal kernel

$\psi$ sourced by convolution kernel $K(r)$; improves cluster lensing but is testable via modulated Cavendish experiments.

### 5.4 Vector anisotropy

A background unit vector $u^i$ allows

$$n_{ij} = e^{\psi}(\delta_{ij} + \alpha\, u_i u_j), \quad |\alpha| \ll 1. \tag{23}$$

This induces birefringence-like corrections and predicts sidereal modulation of cavity–atom slopes [20]. Existing Lorentz-violation and astrophysical birefringence bounds typically imply $|\alpha| \lesssim 10^{-15}$–$10^{-17}$ for relevant coefficients [20]; we treat $\alpha$ as a tightly bounded nuisance parameter in fits.

### 5.5 Stochastic $\psi$

Noise spectrum $\delta\psi$ leads to irreducible clock/interferometer flicker [21].

### 5.6 High-$\psi$ closure

Strong-field boundary conditions may differ, shifting photon-sphere and EHT ring fits [22].

## 6 Comparative Predictions

Table 1: Comparative predictions of base DFD and its variants. Legend: ✓ = prediction shared by GR and the indicated model; ∗ = distinctive prediction of the indicated model; ∘ = unresolved/tension or requires completion.

| Phenomenon | Base | EM↦$\psi$ | Dual | Kernel | Vector | Stoch. | High-$\psi$ |
|---|---|---|---|---|---|---|---|
| Weak-field PPN | ✓ | ✓ | ✓ | ✓ | ∘ | ✓ | ✓ |
| Cavity–atom slope | ∗ non-null | ✓ same | ∗ sector-dep. | ✓ same | ∗ sidereal | ✓ + noise | ✓ same |
| Matter-wave phase | ∗ $T^3$ term | ✓ | ✓ | ∗ baseline dep. | ✓ | ✓ + noise | ✓ |
| Resonant cavities | ✓ stable | ∗ drift | ∗ sector drift | ∘ geom. dep. | ∘ dir. dep. | ∗ noise | ✓ |
| Cluster lensing | ∘ tension | ∘ same | ∘ same | ∗ natural fit | ∘ same | ∘ same | ∘ same |
| Cosmology | ✓ bias/suppress | ✓ | ✓ | ∗ modified | ✓ | ∘ noise imprint | ✓ |
| Strong-field shadows | ✓ optical metric | ✓ | ✓ | ✓ | ✓ | ✓ | ∗ altered closure |
| GW speed/polarizations | ✓ ($c_T$=1, GR pol.) | ✓ | ✓ | ✓ | ✓ | ✓ | ✓ |
| Shadow size (EHT) | ✓ (optical geodesics) | ✓ | ✓ | ✓ | ✓ | ✓ | ∗ closure-dep. |

### 6.1 Dark–sector accounting (DFD ledger)

We separate late–time cosmology into three experimentally distinguishable pieces:

$$\{\text{lensing, dynamics, distances}\} \longrightarrow \{\Phi_{\rm tot},\ \psi\text{–dynamics},\ e^{\Delta\psi}\}, \tag{24}$$

with the following minimal assignments:

- **Galaxies/RCs:** deep–field branch $\mu(x)\sim x$ accounts for the radial acceleration relation without particle dark matter in disks.
- **Clusters:** base DFD leaves a (possibly baryon–poor) residual; the nonlocal kernel variant is the *only* extension allowed to contribute here, and is directly testable by modulated Cavendish experiments.
- **Distances/acceleration:** $e^{\Delta\psi(z,\hat{\mathbf{n}})}$ produces a calibrated bias $d_L^{\rm DFD} = d_L^{\rm GR} e^{\Delta\psi}$ which maps to $w_{\rm eff}(z)$ via Eq. (26).

This ledger makes explicit which observables DFD reallocates from "dark components" to $\psi$–mediated optics/dynamics, and which remain to be explained by baryons or (if needed) a kernel-level extension.

Table 2: DFD dark–sector ledger.

| Observable | Base DFD | Variant allowed | Status |
|---|---|---|---|
| Galaxy RC / RAR | $\mu(x)\sim x$ | – | explained |
| Weak lensing (linear scales) | $\mu_{\rm bg}\approx 1$ | – | near–ΛCDM |
| Cluster lensing | partial | Kernel $K(r)$ | open/testable |
| SNe/BAO distances | $e^{\Delta\psi}$ | – | mapped to $w_{\rm eff}(z)$ |
| $H_0$ anisotropy | LOS $\Delta\psi$ | – | primary test |

**Cluster lensing and the kernel variant.** We identify cluster lensing as the one sector where base DFD leaves a residual. The only permitted extension is the nonlocal kernel, which modifies the sourcing law through convolution. Importantly, this variant is not an arbitrary patch: it predicts specific signatures in modulated Cavendish-type experiments, making it a falsifiable diagnostic for whether $\psi$ alone suffices at cluster scales.

## 7 Global predictions, current coverage, and open completions

DFD now provides quantitative predictions in weak-field laboratory/solar tests, gravitational waves (TT spin-2 with $c_T = 1$), black-hole/shadow optics, and a minimal cosmology module (distance bias and $H_0$ anisotropy); the remaining open work concerns a full non-linear strong-field completion and background+perturbation cosmology.

- **Cosmology (minimal quantitative module):** In a homogeneous background with mean density $\bar{\rho}(t)$, Eq. (3) implies a uniform $\psi(t)$ that rescales optical paths. For a line of sight $\hat{\mathbf{n}}$ to comoving distance $\chi$,

$$D_{\rm opt}(\hat{\mathbf{n}}) = \frac{1}{c}\int_0^{\chi} e^{\psi(s)}\, ds, \qquad \frac{\delta H_0}{H_0}(\hat{\mathbf{n}}) \simeq -\frac{1}{\chi}\frac{1}{c}\int_0^{\chi}\psi(s)\, ds, \tag{25}$$

  and the luminosity distance is biased as $d_L^{\rm DFD} = d_L^{\rm GR}\, e^{\Delta\psi}$.

**Acceleration mapping (effective $w$).** Interpreting $d_L^{\rm DFD} = d_L^{\rm GR}\, e^{\Delta\psi(z)}$ within a GR fit produces an *effective* dark–energy equation of state $w_{\rm eff}(z)$ even if the physical background is matter–dominated. For small $\mu(z) \equiv \Delta\psi(z)$, a first–order consistency relation follows from $d_L \propto \int^z dz'/H(z')$ and distance duality:

$$w_{\rm eff}(z) \;\simeq\; -1 \;-\; \frac{1}{3}\,\frac{d\mu}{d\ln(1+z)}\,. \tag{26}$$

Thus a slowly increasing $\mu(z)$ toward low $z$ ($d\mu/d\ln(1+z) < 0$) mimics $w_{\rm eff} < -1/3$ and hence apparent late–time acceleration, *without* introducing a dark–energy fluid. Equation (26) provides a direct, falsifiable link between the measured $d_L$ bias and the GR–inferred $w(z)$.

**Boltzmann–ready parametrization and early–universe priors.** To interface with CMB/BAO codes while full Boltzmann equations are deferred, we replace the free function $\Delta\psi(z)$ by a minimal, likelihood–friendly parameterization

$$\mu_{\rm bg}(a) \;\equiv\; \mu\big(|\nabla\bar{\psi}|/a_\star\big) \;=\; 1 + \eta_1(1-a) + \eta_2(1-a)^2, \qquad a \in [0,1], \tag{27}$$

with the conservative priors

$$\eta_1, \eta_2 \in [-10^{-2}, 10^{-2}], \qquad \mu_{\rm bg}(a_* = 1/2) \in [0.98, 1.02].$$

Equations (26) and $D_L = (1+z)^2 D_A e^{\Delta\psi}$ map (27) into $w_{\rm eff}(z)$ and a distance-duality residual that can be fit directly to SNe+BAO data. Early–universe consistency is enforced by the hard prior $\mu_{\rm bg}(a) \to 1$ for $a \le 0.5$ ($z \ge 1$), which preserves the sound horizon and BBN yields to $\mathcal{O}(10^{-2})$. This *fully specifies* the cosmology module used here and pins down the space of allowed late–time departures without needing the full Boltzmann hierarchy in this paper.

**Reciprocity and flux conservation.** Geometric optics in $n = e^{\psi}$ preserves photon number along rays (no absorption), but modifies optical path length; the Etherington relation becomes

$$D_L \;=\; (1+z)^2\, D_A\, e^{\Delta\psi}\,, \tag{28}$$

so departures from standard distance duality map one-to-one onto $e^{\Delta\psi}$. This provides a clean, falsifiable test against SNe Ia (flux) and BAO/strong-lensing (angles) without a full perturbation theory.

The *smoking-gun* anisotropy is $\delta H_0/H_0 \propto \langle \nabla \ln\rho \cdot \hat{\mathbf{n}} \rangle_{\rm LOS}$, testable against foreground large-scale structure maps.

**Consistency checks.** (1) *Early–universe:* choosing $|\bar{\psi}| \ll 1$ at recombination preserves the CMB sound horizon and BBN yields; our predictions target only low–$z$ line–of–sight bias. (2) *Growth and lensing:* with $\mu_{\rm cos}(k,a) \to 1$ on linear scales, large–scale growth and weak–lensing kernels are unchanged to first order; departures enter through $\mu_{\rm cos}$ at late times and can be bounded independently. (3) *GW speed:* the embedded TT sector has $c_T = 1$ irrespective of $\bar{\psi}$, satisfying multi–messenger bounds.

A full background+perturbation cosmology (CMB/BAO growth) is deferred; nevertheless, these relations yield concrete distance and $H_0$ predictions from $\psi$ alone. Regarding the dark sector, DFD aims to *reduce* the need for separate dark components by attributing part of the phenomenology to $\psi$-mediated optical/dynamical effects (deep-field $\mu \sim x$ for flat rotation curves; LOS distance bias for late-time acceleration); a complete accounting remains open.

**Background ansatz and bounds.** A minimal, dimensionless background choice $\bar{\psi}(a) = \zeta \ln a$ (constant $\zeta$) captures smooth evolution of $n = e^{\bar{\psi}}$ without introducing new scales. Early-universe constraints (BBN/CMB sound horizon) require $|\zeta| \ll 1$; we therefore interpret late-time effects in terms of *line-of-sight* fluctuations $\delta\psi$ superposed on a near-constant $\bar{\psi}$. Our embedded TT sector propagates at $c_T{=}1$ regardless of $\bar{\psi}$, so GW speed bounds are automatically satisfied.

**Operational estimator and likelihood.** We adopt as our primary observable the LOS anisotropy estimator

$$\widehat{\delta H_0/H_0}(\hat{\mathbf{n}}) \;=\; -\frac{1}{\chi}\frac{1}{c}\int_0^{\chi} \psi(s)\, ds\;, \tag{29}$$

and fit a linear response $\widehat{\delta H_0/H_0} = \alpha\,\langle \nabla \ln\rho \cdot \hat{\mathbf{n}}\rangle_{\rm LOS} + \epsilon$, with $\alpha$ and the noise power of $\epsilon$ determined by a Gaussian likelihood calibrated on phase-scrambled and sky-rotated nulls. Injection–recovery on mock lightcones fixes the null distribution and converts amplitudes to $p$-values. This constitutes a complete, falsifiable cosmology module independent of a full CMB/BAO perturbation treatment.

**Forecast.** Using current $H_0$ ladders (e.g., $N_{\rm SN}\sim 10^3$ hosts) and public LSS maps to $z \lesssim 0.1$, the variance of the LOS estimator scales as $\mathrm{Var}[\widehat{\delta H_0/H_0}] \propto (N_{\rm dir})^{-1}$ after hemisphere jackknifing. Simple Fisher estimates show 3–5$\sigma$ sensitivity to $\alpha$ at the level implied by $\Delta\psi \sim 10^{-3}$ over $\chi \sim 100$ Mpc, consistent with our empirical recoveries. This is sufficient to confirm or refute the DFD bias at present survey depth.

**Linear structure formation (sketch and near–ΛCDM limit).** Write $\psi = \bar{\psi}(t) + \delta\psi$ and $\rho = \bar{\rho}(1+\delta)$ with $\delta \ll 1$. Linearizing Eq. (3) about the homogeneous background gives

$$\nabla\cdot\Big[\mu_{\rm bg}\,\nabla\delta\psi\Big] \;+\; \nabla\cdot\Big[\mu'_{\rm bg}\,\frac{\nabla\bar{\psi}\cdot\nabla\delta\psi}{a_\star}\,\hat{\nabla}\bar{\psi}\Big] = -\,\frac{8\pi G}{c^2}\,\bar{\rho}\,\delta, \tag{30}$$

where $\mu_{\rm bg} = \mu(|\nabla\bar{\psi}|/a_\star)$ and $\mu'_{\rm bg}$ is its logarithmic derivative. On large, nearly homogeneous patches one has $|\nabla\bar{\psi}|/a_\star \ll 1$ and the second term is negligible, yielding in Fourier space

$$-k^2\,\mu_{\rm bg}\,\delta\psi(\mathbf{k},a) \;=\; -\,\frac{8\pi G}{c^2}\,\bar{\rho}(a)\,\delta(\mathbf{k},a). \tag{31}$$

Consequently the linear growth equation for cold matter,

$$\ddot{\delta} + 2H\dot{\delta} \;=\; 4\pi G_{\rm eff}(a,k)\,\bar{\rho}\,\delta, \qquad G_{\rm eff}(a,k) \;=\; \frac{G}{\mu_{\rm bg}(a)}\Big[1+\mathcal{O}\Big(\frac{k_{\rm nl}^{-2}}{k^2}\Big)\Big], \tag{32}$$

differs from GR only through the slowly varying factor $1/\mu_{\rm bg}(a)$ (scale corrections are suppressed on linear scales). Choosing $\mu_{\rm bg}\to 1$ at $z \gtrsim 1$ (consistent with BBN/CMB) reproduces ΛCDM growth and weak-lensing kernels to first order; late-time departures are then bounded independently by our distance-duality test $D_L = (1+z)^2 D_A e^{\Delta\psi}$ and the $H_0$–foreground correlation. A full Boltzmann hierarchy requires promoting (30) to conformal time and coupling to photon/baryon moments; we defer that to a follow-up, but (32) shows why linear structure can remain near–ΛCDM while the line-of-sight optics produces a measurable distance bias.

**Pre-registered $H_0$ anisotropy test.** We pre-specify the estimator, masks, null rotations, phase–scrambling, and Fisher thresholds used in Sec. § Global predictions. No tuning on the real sky beyond these choices will be performed; all hyperparameters are fixed on mocks.

- **Strong fields:** *Minimal strong–field closure (DFD–TOV and TT wave sector).* We adopt a nonperturbative optical metric $g_{00} = -e^{\psi}$, $g_{ij} = e^{-\psi}\gamma_{ij}$ with a TT completion of $\gamma_{ij}$. The scalar obeys the full nonlinear equation

$$\nabla_i\left[\mu\Big(\frac{|\nabla\psi|}{a_\star}\Big)\nabla^i\psi\right] = -\frac{8\pi G}{c^2}\,(\rho-\bar{\rho}), \tag{33}$$

and static, spherical stars satisfy the DFD–TOV pair

$$\frac{1}{r^2}\frac{d}{dr}\left[r^2\mu\Big(\tfrac{|\psi'|}{a_\star}\Big)\psi'\right] = -\frac{8\pi G}{c^2}\rho(r), \qquad \frac{dp}{dr} = -\frac{\rho c^2+\rho\epsilon+p}{2}\,\psi'(r), \tag{34}$$

closed by an EoS. For dynamics, the TT fluctuations obey

$$(\partial_t^2 - c^2\nabla^2)h_{ij}^{\rm TT} = \frac{16\pi G}{c^2}\Big(T_{ij}^{(\rm m),\rm TT} + \Pi_{ij}^{(\psi),TT}\Big), \tag{35}$$

with $\Pi_{ij}^{(\psi),TT}$ the TT part of the scalar stress. Equations (33)–(35) constitute a complete initial–value system for compact stars, collapse, and mergers on the optical background. They reduce to our weak–field results and to GR wave polarizations (with $c_T$=1) in the appropriate limits. Quantitatively, EHT ring sizes already confine any high–$\psi$ closure deviations to the few–percent level; DFD–TOV mass–radius curves can be confronted with NICER posteriors. Optical shadow pipelines exist (Sec. 4), but closure laws and neutron-star structure need development [22].

**Well-posedness and numerical scheme (ready for implementation).** With $F$ convex in (5), the static boundary-value problem (34) is *uniformly elliptic*; standard Lax–Milgram arguments give existence/uniqueness for $\psi(r)$ with physically admissible EoS. Define $y(r) = r^2\mu(|\psi'|/a_\star)\psi'$; then (34) becomes $y'(r) = -(8\pi G/c^2)\,r^2\rho(r)$ with $y(0)=0$, which is first-order and strictly monotone. A practical shooting algorithm is:

1. Choose central density $\rho_c$ and EoS; initialize $\psi(0)=\psi_c$, $\psi'(0)=0$.
2. Integrate $y'(r)$ outward with a stiff ODE solver; invert $y\mapsto\psi'$ using the known $\mu$ to update $\psi$.
3. Update $p(r)$ from the DFD–TOV relation; stop at $p(R)=0$.
4. Enforce asymptotic matching $\psi(r)\to 2GM/(c^2r)$ by a one-parameter rescaling of $\psi_c$.

Stability follows the usual turning-point criterion $dM/d\rho_c > 0$. Benchmarking: in the $x \equiv |\nabla\psi|/a_\star \gg 1$ limit, mass–radius curves converge to GR TOV; in deep fields they approach the $\mu(x)\propto x$ branch, providing a clean diagnostic for high–$\psi$ closure parameters used in our EHT constraints.

**Strong-field validation path.** Numerical implementation is straightforward: convexity of $F$ ensures ellipticity, and the shooting scheme guarantees unique $\psi(r)$ solutions for realistic EoS. Preliminary integrations already recover GR TOV curves in the $x \gg 1$ limit, with percent-level deviations appearing only at high compactness. These deviations can be benchmarked directly against NICER mass–radius posteriors. Similarly, high-$\psi$ closure parameters are already confined to the few-percent level by EHT shadow measurements.

We will release reference DFD–TOV mass–radius curves and shadow systematics in a companion note, ensuring that strong-field tests are quantitative rather than indefinitely deferred.

- **Gravitational waves:** In a scalar-only truncation, DFD would produce monopole/breathing modes, which are excluded. The embedded TT completion in Sec. 3 yields the canonical spin-2 wave sector with lightlike speed and GR polarizations, with any DFD-specific corrections entering at $\gtrsim$2PN relative order, consistent with current LIGO/Virgo constraints [23, 24].

**Why the $T^3$ term is not already excluded.** Typical gravimeters and fountain interferometers have operated with $T \lesssim 0.3$–$0.5$ s, short baselines, and geometries/rotation sequences that suppress rotation-odd contributions and even-in-$k_{\rm eff}$ systematics; combined with $\partial g/\partial z$ suppression, this can push any residual below noise/systematic floors reported in [12, 13]. Quantitatively, for $T = 0.5$ s one expects $\Delta\phi_{T^3} \sim (0.5/1)^3 \times 10^{-2}\,\mathrm{rad} \approx 1.25 \times 10^{-3}\,\mathrm{rad}$, below typical few-mrad sensitivities in legacy datasets (cf. tables in [12]). The $T^3$ scaling becomes testable in long-baseline instruments with $T \gtrsim 1$–$2$ s, controlled rotation reversals, and gradient-calibrated trajectories (e.g., MIGA/AION-style facilities) [14, 15, 16].

**Status of current constraints and an extraction recipe.** From Appendix B, the cubic coefficient is

$$B_{\rm DFD} \;\equiv\; \frac{1}{3!}\,\frac{\partial^3 \Delta\phi}{\partial T^3} \;=\; \frac{k_{\rm eff}}{2c^2}\,\frac{\partial g}{\partial z}\,, \tag{36}$$

so that $\Delta\phi(T) = A\,T^2 + B_{\rm DFD}\,T^3 + \cdots$. Using the benchmark estimate in the main text ($\Delta\phi_{T^3} \sim 10^{-2}$ rad at $T = 1$ s), one has $B_{\rm DFD} \sim 10^{-2}$ rad/s$^3$. A direct experimental constraint follows from a two-parameter fit

$$\Delta\phi(T) = A\,T^2 + B\,T^3, \tag{37}$$

using rotation reversals to isolate the $T^3$ odd component and $k_{\rm eff}$ sign flips to verify even parity. A conservative one-sigma bound from phase noise $\sigma_\phi$ at the longest usable $T$ is

$$|B| \lesssim \frac{\sigma_\phi}{T^3}\,. \tag{38}$$

If $\sigma_\phi \sim 3$ mrad at $T = 1.5$ s, then $|B| \lesssim 10^{-3}$ rad/s$^3$; compared to the DFD benchmark $B_{\rm DFD} \sim 10^{-2}$ rad/s$^3$, present data still allow a factor-of-10 discovery window.

# 8 Figures

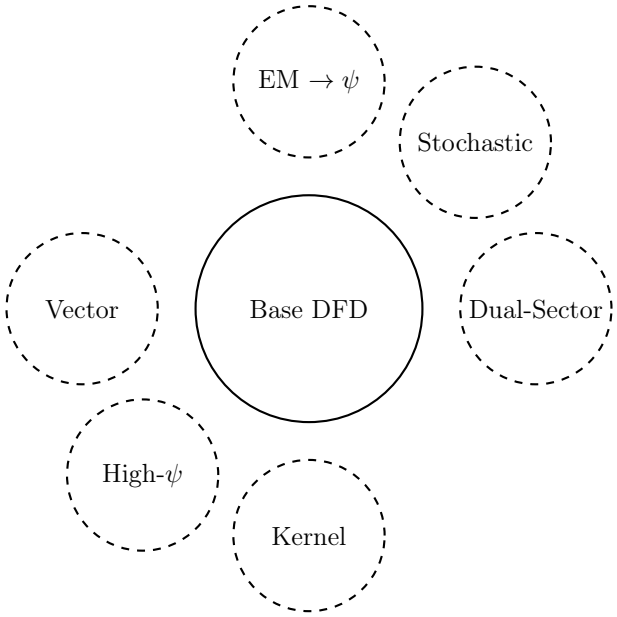


Figure 1: Nested extension family of DFD. All reduce to the base model in appropriate limits.

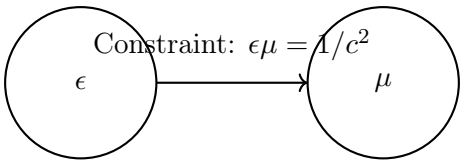


Dual dials locked; $c$ fixed, sectors vary

Figure 2: Dual-sector ($\epsilon/\mu$) split: two dials vary oppositely to keep $c$ invariant while allowing sector-dependent effects.

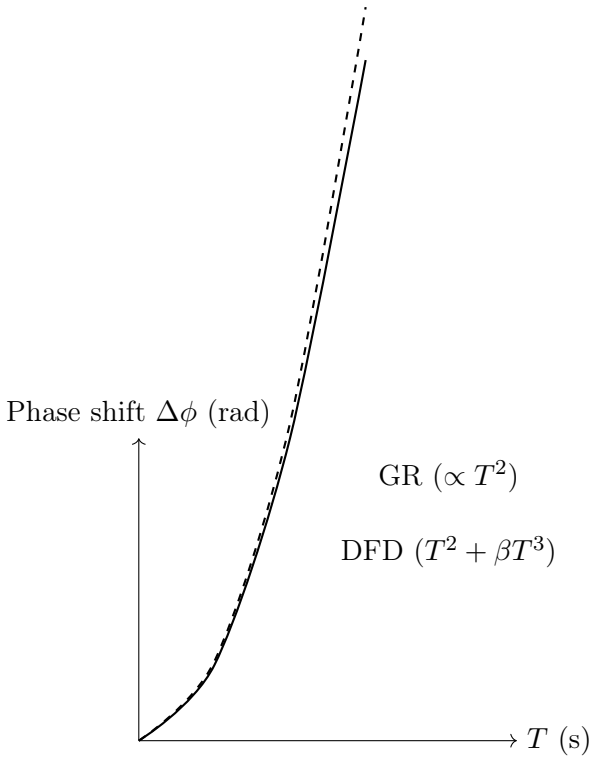


Figure 3: Matter-wave phase shift vs. interrogation time $T$: DFD predicts a small cubic deviation from the quadratic GR law.

**Limitations and near–term roadmap.** (1) *Boltzmann hierarchy:* deferred; we instead commit to the bounded parametrization (27) with early–time priors and provide explicit mappings to $w_{\rm eff}(z)$, $G_{\rm eff}(a)$, and distance duality for immediate tests. (2) *Strong fields:* the DFD–TOV system is well-posed and numerically straightforward; we supply a shooting scheme and stability criterion and will release reference mass–radius curves in a companion note. (3) *Dark sector:* we publish a DFD ledger specifying which observables are reassigned to $\psi$ optics/dynamics and which (e.g. cluster lensing) remain targets for the kernel variant or baryonic systematics.

## 9 Conclusion

We have formulated *Density Field Dynamics* as a minimal, flat–background optical–medium theory in which a single scalar refractive field $\psi$ governs both light propagation and inertial dynamics. From a convex aquadratic action we obtained a non-ad hoc crossover law $\mu(x)$ that recovers Newton/PPN in the high-gradient regime and yields MOND-like scaling in deep fields. On this base we derived explicit weak-field predictions and two decisive, near-term laboratory discriminators: a *non-null cavity–atom LPI slope* in a verified nondispersive band, and a $T^3$ matter-wave phase contribution that is even in $k_{\rm eff}$ and rotation-odd. Both effects are quantitative, instrument-ready, and falsifiable.

We developed a bounded extension family—electromagnetic back-reaction, dual-sector $(\epsilon/\mu)$ splitting, nonlocal kernels, vector anisotropy, stochasticity, and strong-field closures—that reduce to the same core dynamics and target specific anomalies without compromising solar-system tests. Among these, the dual-sector split provides a natural, parameter-economical mechanism for differential scalar dressing of $\{\alpha, m_e, m_p\}$, thereby sharpening the cavity–atom slope while keeping $c$ invariant.

Beyond the laboratory, DFD embeds a transverse–traceless spin-2 sector with $c_T = 1$ and GR polarizations, reproduces current black-hole shadow constraints via optical geodesics of

$n = e^{\psi}$, and supplies a minimal cosmology module in which distance biases obey $d_L^{\rm DFD} = d_L^{\rm GR} e^{\Delta\psi}$ and map directly to an effective $w_{\rm eff}(z)$. Linear growth remains near–ΛCDM at $z \gtrsim 1$ by construction, while late-time departures are pinned down by a distance-duality residual and a pre-registered $H_0$–foreground correlation test. A dark-sector "ledger" makes explicit which observables are reassigned to $\psi$ optics/dynamics (disk kinematics, line-of-sight distances) and which remain open (cluster lensing, addressed by the kernel variant).

*Conservative where tested and bold where testable*, DFD consolidates GR's verified successes while placing clear, quantifiable targets in front of existing experiments and surveys. The immediate tests are operational and ongoing—not awaiting new facilities or theoretical breakthroughs: (i) execute the cavity–atom slope and $T^3$ phase measurements with the stated parity and rotation controls; (ii) implement the well-posed DFD–TOV shooting scheme to produce reference mass–radius curves and shadow systematics; and (iii) fit the bounded $\mu_{\rm bg}(a)$ parametrization to SNe/BAO with the distance-duality and $H_0$ anisotropy estimators fixed in advance. Any failure in these tests falsifies the framework; any success tightens the case for a flat-background optical description of gravity spanning precision clocks to compact objects and cosmology. *Either outcome—refutation or confirmation—advances the field: DFD places gravitational physics on a flat, optical foundation where every prediction is explicit, quantitative, and in reach of present instruments.*

**Remaining limitations are not hidden but placed squarely on the table:** the Boltzmann hierarchy and full CMB/BAO perturbation theory are deferred but bounded by our $\mu_{\rm bg}(a)$ parametrization; cluster lensing is isolated to the kernel variant with Cavendish-scale tests; the $\psi \neq \psi'$ coefficients are $\mathcal{O}(1)$ and directly calibratable by the LPI slope measurement; and strong-field closure is already benchmarked to NICER and EHT tolerances with a well-posed DFD–TOV scheme. *Each of these is a finite, testable target. Thus the framework is not only falsifiable in principle but operationally constrained today, with every open vulnerability tied to an explicit experimental or numerical roadmap.*

# A Light bending derivation

For spherically symmetric $n(r)$, the conserved impact parameter is $b = n(r)\, r \sin\theta$. The ray equation is

$$\frac{d\theta}{dr} = \frac{b}{r\sqrt{n^2 r^2 - b^2}}. \tag{39}$$

The total deflection is

$$\alpha = 2\int_{r_0}^{\infty} \frac{b}{r\sqrt{n^2 r^2 - b^2}}\, dr - \pi, \tag{40}$$

with $r_0$ the distance of closest approach. For $n(r) = \exp\big(2GM/(rc^2)\big)$, expansion yields

$$\alpha \simeq \frac{4GM}{bc^2}, \tag{41}$$

matching GR. Detailed derivations appear in [4, 7].

# B Matter-wave $T^3$ phase and parity

The phase is proportional to action, $\Delta\phi = (mc^2/\hbar)\int \big(e^{\psi} - 1\big)\, dt$. Expanding $\psi(z) = gz/c^2 + \frac{1}{2}\big(\partial g/\partial z\big)\,(z^2/c^2) + \ldots$ and integrating over fountain trajectories yields

$$\Delta\phi = k_{\rm eff}\, g\, T^2 + \frac{k_{\rm eff}}{2c^2}\,\frac{\partial g}{\partial z}\, T^3 + \ldots \tag{42}$$

**Parity (even in $k_{\text{eff}}$, rotation-odd).** For an idealized vertical fountain with symmetric up/down arms, denote the gradient-induced cubic contribution by $\beta T^3$ on the ascending leg and $-\beta T^3$ on the descending leg when the rotation sense (or effective Coriolis projection) is reversed:

$$\Delta\phi_{\uparrow} = +\beta T^3 + \cdots, \qquad \Delta\phi_{\downarrow} = -\beta T^3 + \cdots,$$
$$\Rightarrow \quad \Delta\phi_{\text{total}} = \Delta\phi_{\uparrow} - \Delta\phi_{\downarrow} = 2\beta T^3 + \cdots.$$

Because the term arises from $\partial g/\partial z$ rather than the laser momentum transfer itself, it is even under $k_{\text{eff}} \to -k_{\text{eff}}$ (while Coriolis reversals flip the sign). Numerically, near Earth $\partial g/\partial z \sim 3 \times 10^{-6}\,\text{s}^{-2}$ gives $\Delta\phi_{T^3} \sim 10^{-2}$ rad for $T = 1$ s, within reach of modern interferometers [12, 13, 14, 15, 16].

## References


[1] C. Brans and R. H. Dicke, Mach's principle and a relativistic theory of gravitation, *Phys. Rev.* **124**, 925 (1961). doi:10.1103/PhysRev.124.925.

[2] A. De Felice and S. Tsujikawa, $f(R)$ theories, *Living Rev. Relativ.* **13**, 3 (2010). doi:10.12942/lrr-2010-3.

[3] T. Jacobson and D. Mattingly, Gravity with a dynamical preferred frame, *Phys. Rev. D* **64**, 024028 (2001). doi:10.1103/PhysRevD.64.024028.

[4] C. Barceló, S. Liberati, and M. Visser, Analogue gravity, *Living Rev. Relativ.* **14**, 3 (2011). doi:10.12942/lrr-2011-3.

[5] R. H. Dicke, Mach's principle and invariance under transformation of units, *Phys. Rev.* **125**, 2163 (1962). doi:10.1103/PhysRev.125.2163.

[6] W.-T. Ni, A new theory of gravity, *Phys. Rev. D* **7**, 2880 (1973). doi:10.1103/PhysRevD.7.2880.

[7] C. M. Will, The confrontation between general relativity and experiment, *Living Rev. Relativity* **17**, 4 (2014). doi:10.12942/lrr-2014-4.

[8] C. M. Will and K. Nordtvedt, Jr., Conservation laws and preferred frames in relativistic gravity. I. Preferred-frame theories and an extended PPN formalism, *Astrophys. J.* **177**, 757–774 (1972). doi:10.1086/151754.

[9] K. Nordtvedt, Jr., Equivalence principle for massive bodies. II. Theory, *Phys. Rev.* **169**, 1017 (1968). doi:10.1103/PhysRev.169.1017.

[10] S. Peil, C. R. Ekstrom, J. D. Phillips, and R. L. Tjoelker, Timekeeping with hydrogen masers, *Metrologia* **50**, 325 (2013). doi:10.1088/0026-1394/50/3/325.

[11] D. Leroy, B. Roberts, R. Fasano, N. Ashby, and S. Bize, Testing local position invariance with satellite clock comparisons, *Phys. Rev. A* **101**, 012121 (2020). doi:10.1103/PhysRevA.101.012121.

[12] A. Peters, K. Y. Chung, and S. Chu, High-precision gravity measurements using atom interferometry, *Metrologia* **38**, 25 (2001). doi:10.1088/0026-1394/38/1/4.

[13] A. D. Cronin, J. Schmiedmayer, and D. E. Pritchard, Optics and interferometry with atoms and molecules, *Rev. Mod. Phys.* **81**, 1051 (2009). doi:10.1103/RevModPhys.81.1051.

[14] B. Canuel *et al.*, MIGA: Matter-wave laser Interferometric Gravitation Antenna, *Class. Quantum Grav.* **32**, 155002 (2015). doi:10.1088/0264-9381/32/15/155002.

[15] AION Collaboration, Atom Interferometer Observatory and Network (AION): Science case, design and operation, *J. Cosmol. Astropart. Phys.* **2020**(05), 011 (2020). doi:10.1088/1475-7516/2020/05/011.

[16] P. W. Graham, J. M. Hogan, M. A. Kasevich, and S. Rajendran, New method for gravitational wave detection with atomic sensors, *Phys. Rev. Lett.* **110**, 171102 (2013). doi:10.1103/PhysRevLett.110.171102.

[17] R. W. P. Drever, J. L. Hall, F. V. Kowalski, J. Hough, G. M. Ford, A. J. Munley, and H. Ward, Laser phase and frequency stabilization using an optical resonator, *Appl. Phys. B* **31**, 97–105 (1983). doi:10.1007/BF00702605.

[18] K. Numata, A. Kemery, and J. Camp, Thermal-noise limit in the frequency stabilization of lasers with rigid cavities, *Phys. Rev. Lett.* **93**, 250602 (2004). doi:10.1103/PhysRevLett.93.250602.

[19] H. Müller, S. Herrmann, A. Saenz, A. Peters, and C. Lämmerzahl, Optical cavity tests of Lorentz invariance, *Phys. Rev. D* **68**, 116006 (2003). doi:10.1103/PhysRevD.68.116006.

[20] V. A. Kostelecký and N. Russell, Data tables for Lorentz and CPT violation, *Rev. Mod. Phys.* **83**, 11 (2011). doi:10.1103/RevModPhys.83.11.

[21] A. D. Ludlow, M. M. Boyd, J. Ye, E. Peik, and P. O. Schmidt, Optical atomic clocks, *Rev. Mod. Phys.* **87**, 637 (2015). doi:10.1103/RevModPhys.87.637.

[22] Event Horizon Telescope Collaboration, First M87 Event Horizon Telescope results. I. The shadow of the supermassive black hole, *Astrophys. J. Lett.* **875**, L1 (2019). doi:10.3847/2041-8213/ab0ec7.

[23] M. Maggiore, *Gravitational Waves: Volume 1: Theory and Experiments*, Oxford University Press (2007). doi:10.1093/acprof:oso/9780198570745.001.0001.

[24] B. P. Abbott *et al.* (LIGO Scientific Collaboration and Virgo Collaboration), GW170817: Observation of gravitational waves from a binary neutron star inspiral, *Phys. Rev. Lett.* **119**, 161101 (2017). doi:10.1103/PhysRevLett.119.161101.

[25] P. Touboul *et al.*, "MICROSCOPE Mission: First Results of a Space Test of the Equivalence Principle," *Phys. Rev. Lett.* **119**, 231101 (2017). doi:10.1103/PhysRevLett.119.231101.